CHAPTER IV
RESULTS AND DISCUSSION

4.1 Catalyst Characterizations

4.1.1 Thermal Gravimetric Analysis (TGA)

The TG-DTG technique was used to study the thermal decomposition behavior of the prepared catalysts and to obtain their suitable calcination temperature. Figure 4.1 shows the TG-DTG profile of the prepared, Cu-Mo/Al_2O_3 catalyst. The DTG curves consisted of two main exothermic peaks. The first exothermic peak, appeared below 150 °C, is attributed to the removal of physisorbed water molecules. The second exothermic peak between 150 and 350 °C is attributed to the decomposition of unwanted metal precursor. Similar to Cu-Mo/Al_2O_3, other prepared catalysts also exhibited the end of weight loss below 500 °C (Appendix A). Therefore, all the prepared catalysts in this study were calcined at 500 °C.

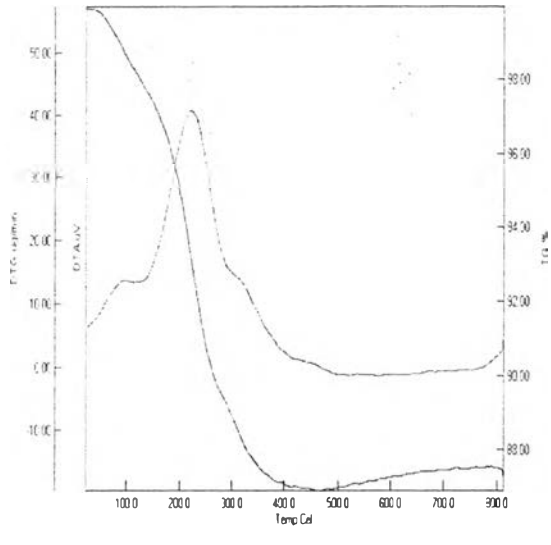

Figure 4.1 TG-DTG profile of prepared Cu-Mo/Al_2O_3.

4.1.2 Temperature Programmed Reduction (TPR)

The temperature programmed reduction technique was used to investigate the reduction behaviors of the prepared catalysts. The TPR profiles of Ni-based, Cu-based, and noble metal catalysts are shown in Figures 4.2-4.4, respectively.

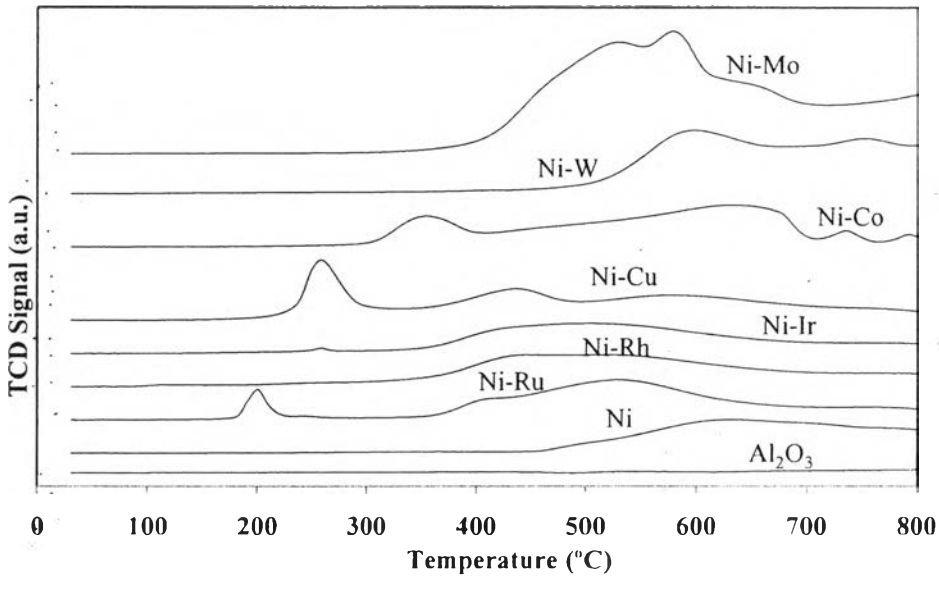

Figure 4.2 TPR profiles of nickel-based catalysts compared with alumina support.

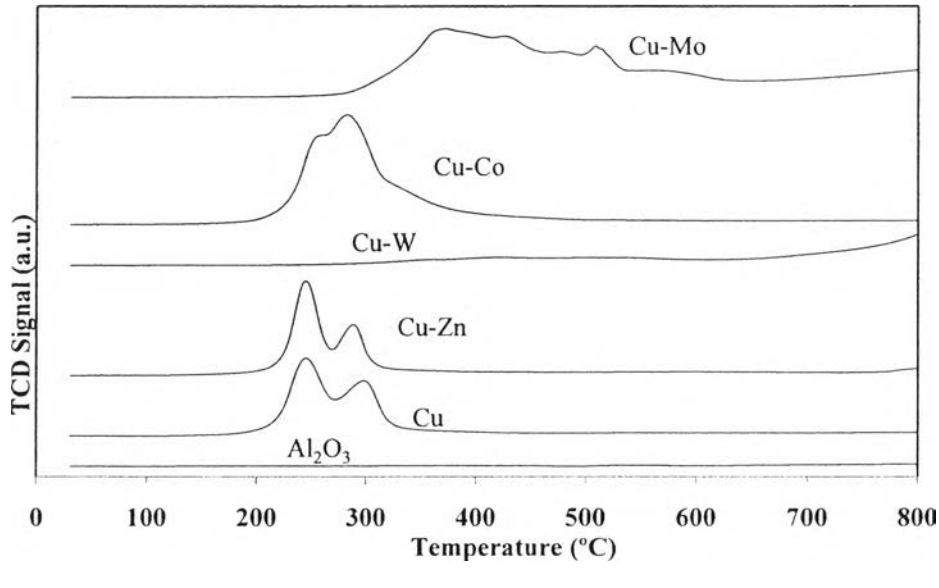

Figure 4.3 TPR profiles of copper-based catalysts compared with alumina support.

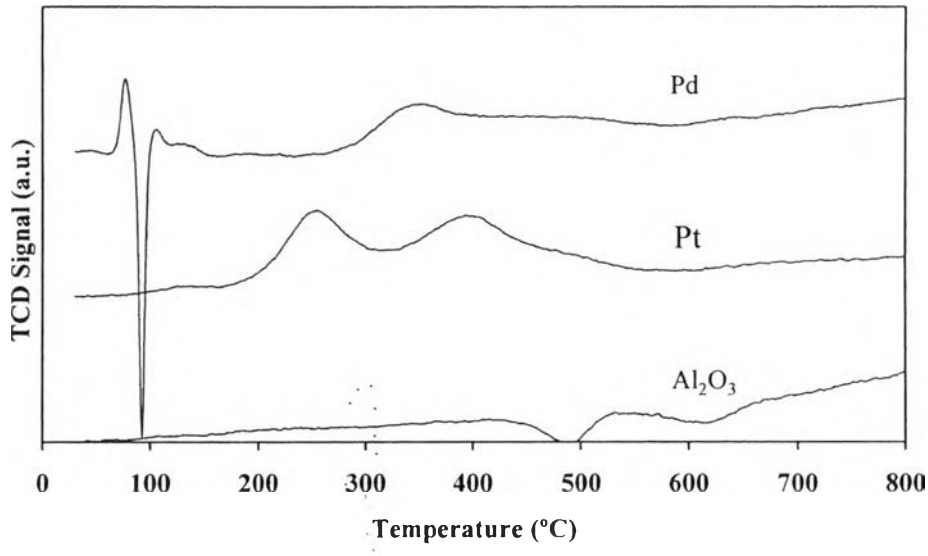

Figure 4.4 TPR profiles of Pt/Al_2O_3 ,Pd/Al_2O_3 compared with alumina support.

The monometallic Ni/Al_2O_3 showed a reduction peak at 600 °C, corresponding to the reduction of NiO which strongly interact with alumina support (Rynkowski *et al.*, 1993). The addition of second metals resulted in lower nickel oxide reduction temperatures. The lower reduction temperature could be because the presence of second metals that were reduced at lower temperatures. It helped catalyze the reduction of nickel oxide.

The $Ni\text{-}Ru/Al_2O_3$, $Ni\text{-}Cu/Al_2O_3$, and $Ni\text{-}Ir/Al_2O_3$ catalysts showed a positive peak at 200, 250, and 260 °C, indicating reduction temperature of the corresponding second metals, respectively.

For Cu-based catalysts, the monometallic Cu showed two reduction peak at 250 and 300 °C which corresponded to the reduction of highly dispersed CuO (Lopez-Suarez *et al.*, 2008). For Cu-Zn and $Cu\text{-}Co/Al_2O_3$ catalysts, the TPR pattern consisted of two reduction peaks at 260 and 290 °C belong to the presence of Zn and Co that could reduce the reduction temperature. In addition, shoulder at 320 °C of TPR pattern of Cu-Co catalysts was associated with the reduction of Co specie.

In case of $Cu\text{-}Mo/Al_2O_3$, positive peak at 370 °C and 447 °C were observed, indicating the Cu associated with Mo.

For Pt/Al_2O_3, the TPR pattern consisted of a small peak at 150 °C and two main reduction peaks at 257 and 395 °C. The small peak at low temperature was attributed to the reduction of PtO_2 species. The two peaks at 257 and 395 °C could be assigned to the reduction of $PtAl_2O_4$ species (Hwang and Yeh, 1996) and two-dimensional phase, with a strong interaction with alumina, respectively (Navarro *et al*, 2005).

Table 4.1 The suitable reduction temperature for each catalyst

Prepared catalysts	Suitable reduction temperature (°C)
Ni-based catalysts	
Ni	630
Ni-Mo	570
Ni-Co	630
Ni-Cu	570
Ni-W	600
Ni-Ru	520
Ni-Rh	485
Ni-Ir	485
Cu-based catalysts	
Cu	293
Cu-Mo	364
Cu-Co	277
Cu-W	515
Cu-Zn	283
Noble metal catalysts	
Pt	388
Pd	335

The Pd/Al_2O_3 showed a positive peak at 80 °C and a negative peak at 90 °C. The positive peak represented the reduction of Pd oxide while the negative

peak represented the decomposition of β-PdHx formed during the reduction (Shekar *et al., 2005).* From TPR results, the suitable reduction temperatures for each catalyst are listed in Table 4.1.

4.1.3 Brunauer-Emmett-Tellet Method (BET)

The BET analyses of the prepared Ni-based, Cu-based and noble metal catalysts are given in Tables 4.2 and 4.3. The surface areas of prepared catalysts were lower when compared with the alumina support (S_{BET} 236 m^2/g, pore volume 0.84 cm^3, pore diameter 142 Å). Among the Ni-based catalysts, surface area decreased in the order of $Ni\text{-}Ru/Al_2O_3 > Ni/Al_2O_3 > Ni\text{-}Ir/Al_2O_3 > Ni\text{-}Rh/Al_2O_3 > Ni\text{-}Co/Al_2O_3 > Ni\text{-}Cu/Al_2O_3 > Ni\text{-}Mo/Al_2O_3 > Ni\text{-}W/Al_2O_3$. For the Cu-based catalysts, the surface area decreased in the following order; $Cu/Al_2O_3 > Cu\text{-}Co/Al_2O_3 > Cu\text{-}Zn/Al_2O_3 > Cu\text{-}Mo/Al_2O_3 > Cu\text{-}W/Al_2O_3$. Noticeably, the presence of molybdenum or tungsten as second metals drastically decreased the surface areas and pore volume. This could result from the extra-large size of metal ions which possibly block the pore of alumina. Noble metal catalysts showed relatively high surface area which corresponded to the low metal loading.

Table 4.2 Catalysts surface area, total pore volume and average pore diameter of Ni-based catalysts

Catalyst	S_{BET} (m^2/g)	Total pore volume (cm^3/g)	Avg. pore diameter (Å)
Ni	218.9	0.7271	132.9
Ni-Mo	148.1	0.4901	132.4
Ni-Co	202.6	0.6893	136.1
Ni-Cu	188.2	0.6487	137.9
Ni-W	104.6	0.3286	125.6
Ni-Ru	221.2	0.7410	134
Ni-Rh	202.8	0.6777	133.7
Ni-Ir	210.5	0.6998	133

Table 4.3 Catalysts surface area, total pore volume and average pore diameter of Cu-based and noble metal catalysts

Catalysts	S_{BET} (m^2/g)	Total pore volume (cm^3/g)	Avg. pore diameter (Å)
10%Cu	228.4	0.8007	140.2
10%Cu-5%Mo	141.8	0.5025	141.7
10%Cu-5%Co	202.9	0.6942	136.9
10%Cu-5%W	60.41	0.1914	124.7
10%Cu-5%Zn	192.3	0.6832	142.1
1%Pt	246.5	0.8352	135.5
1%Pd	243	0.8383	138

4.2 Production of Hydrogenated Biodiesel from Beef Fat

4.2.1 Standard Analysis

The chemical standard of products such as dodecane (n-C_{12}), pentadecane (n-C_{15}), hexadecane (n-C_{16}), heptadecane (n-C_{17}), octadecane (n-C_{18}), eicosane (n-C_{20}), hexadecanol, octadecanol, palmitic acid, oleic acid, stearic acid, monoglycerides, diglycerides, and triglycerides were analyzed by gas chromatograph equipped with an FID detector (Agilent 7890) to identify peaks of feed stock, intermediates and products. The chromatograms are shown in Figure 4.5. The retention time and response factor of the standards are shown in Table 4.4.

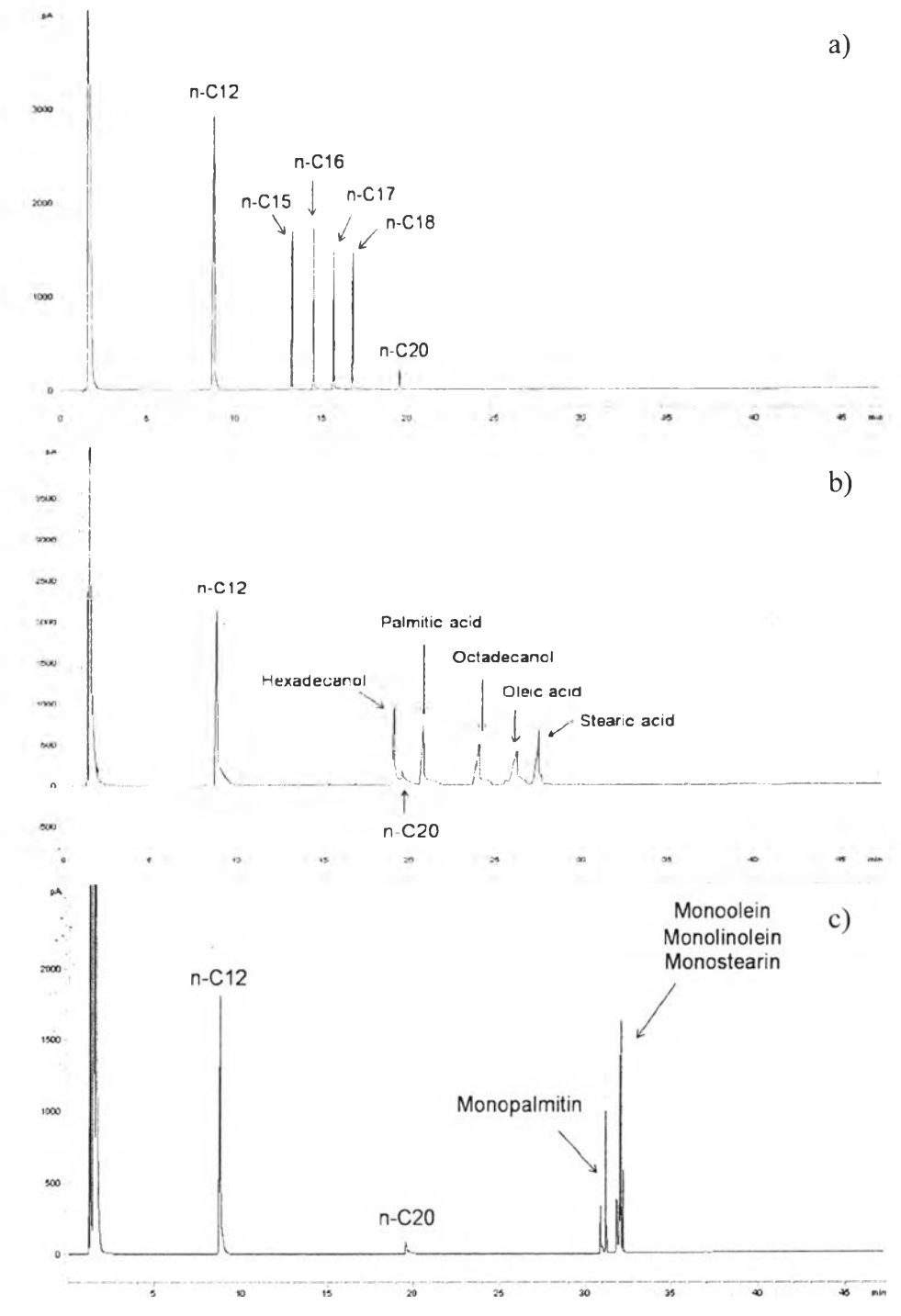

Figure 4.5 Chromatograms of standard chemicals, (a) n-pentadecane, n-hexadecane, n-heptadecane, n-octadecane, (b) hexadecanol, octadecanol, palmitic acid, stearic acid, oleic acid, (c) monoolein, monolinolein, monostearin, monopalmitin, (d) diolein, dilinolein, distearin, dipalmitin, and (e) triolein, trilinolein, tristearin, tripalmitin.

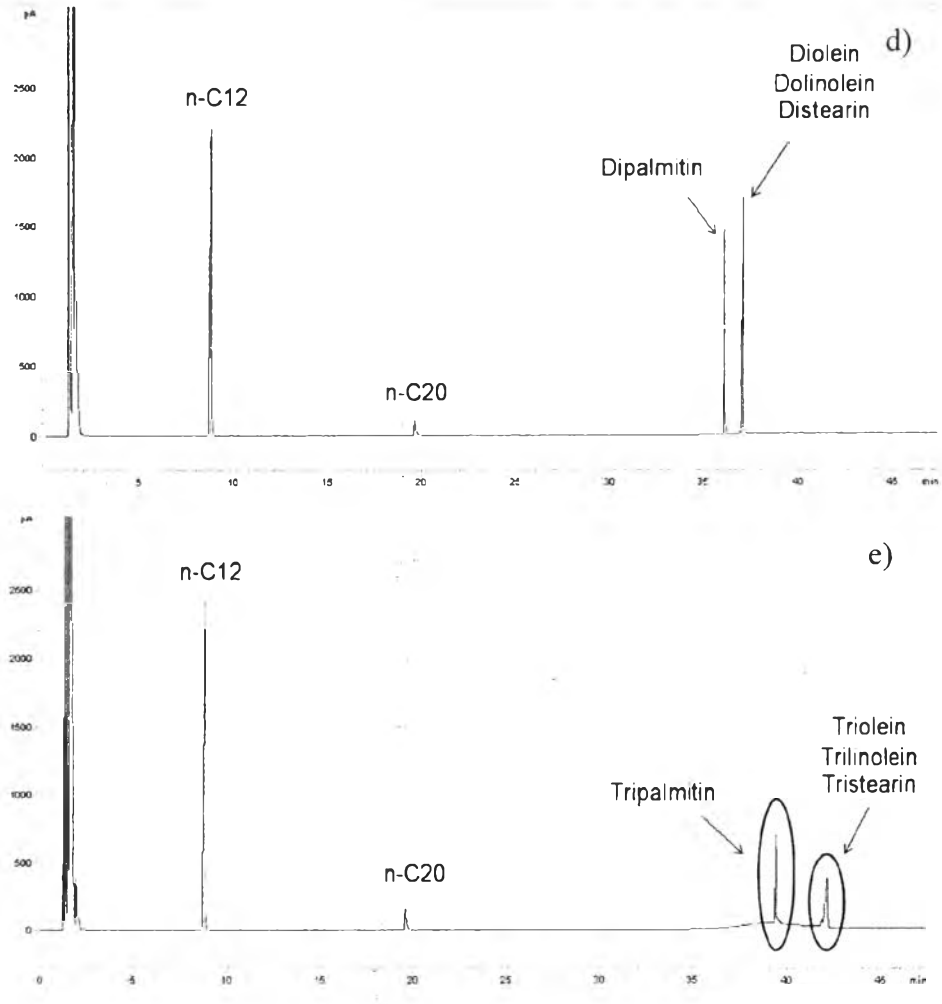

Figure 4.5 (Cont.) Chromatograms of standard chemicals, (a) n-pentadecane, n-hexadecane, n-heptadecane, n-octadecane, (b) hexadecanol, octadecanol, palmitic acid, stearic acid, oleic acid, (c) monoolein, monolinolein, monostearin, monopalmitin, (d) diolein, dilinolein, distearin, dipalmitin, and (e) triolein, trilinolein, tristearin, tripalmitin.

Table 4.4 Retention times and response factors of standard chemicals

Standard chemicals	Retention times	Response factors
Triolein	42.1	0.9913
Trilinolein		
Tristearin		
Tripalmitin	39.4	1.0305
Diolein	37.0	0.9241
Dilinolein		
Distearin		
Dipalmitin	36.0	1.0166
Monoolein	32.2	1.6052
Monolinolein		
Monostearin		
Monopalmitin	31.3	1.5393
Hexadecanol	19.4	0.9994
Octadecanol	24.6	1.2587
Palmitic acid	20.8	1.1796
Stearic acid	27.8	0.9236
Oleic acid	26.1	0.9815
n-Pentadecane	13.5	1.3341
n-Hexadecane	14.8	1.2665
n-Heptadecane	15.9	1.2002
n-Octadecane	17.0	1.1795

4.2.2 Feed Analysis

The beef fat feedstock was analyzed by gas chromatograph to identify its component. The result showed that beef fat contains triglyceride as main component with trace amount of free fatty acid e.g. oleic acid and stearic acid. The GC chromatogram of beef fat is shown in Figure 4.6. Table 4.5 shows the composition of beef fat analyzed by AOAC 966.06. The result indicated that beef fat contained oleic acid as major component, followed by palmitic acid, and stearic acid, respectively. Trace amounts of myristic acid, linoleic acid, myristoleic acid, eicosenoic acid, palmitoleic acid, lauric acid, heptadecanoic acid, were also observed.

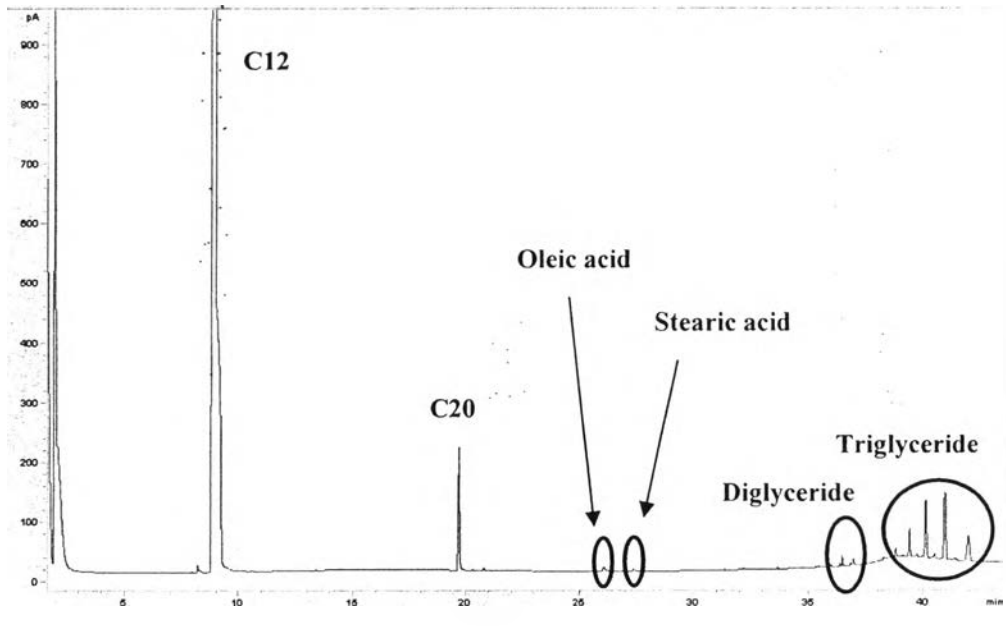

Figure 4.6 Chromatograms of 10% beef fat in dodecane.

Table 4.5 Composition of beef fat investigated in this work

Fatty Acid	Systematic name	Acronym	Formular	M.W.	Composition (wt.%) Beef fat
Caprylic acid	Octanoic acid	8:0	$C_8H_{16}O_2$	144.22	0.02
Capric acid	Decanoic acid	10:0	$C_{10}H_{20}O_2$	172.27	0.05
Lauric acid	Dodecanoic acid	12:0	$C_{12}H_{24}O_2$	200.32	0.11
Myristic acid	Tetradecanoic acid	14:0	$C_{14}H_{28}O_2$	228.38	3.3
	Pentadecanoic acid	15:0	$C_{15}H_{30}O_2$	242.4	0.39
Palmitic acid	Hexadecanoic acid	16:0	$C_{16}H_{32}O_2$	256.43	26.13
	Heptadecanoic acid	17:0	$C_{17}H_{34}O_2$	270.45	0.67
Stearic acid	Octadecanoic acid	18:0	$C_{18}H_{36}O_2$	284.48	18.38
Arachidic acid	-	20:0	$C_{20}H_{40}O_2$	312.53	0.15
Myristoleic acid	-	14:1	$C_{14}H_{26}O_2$	226.36	1.07
Palmitoleic acid	-	16:1	$C_{16}H_{30}O_2$	254.41	0.84
cis-9-Oleic acid	cis-9-Octadecenoic acid	18:1	$C_{18}H_{34}O_2$	282.47	41.71
cis-11-Eicosenoic acid	-	20:1	$C_{20}H_{38}O_2$	310.52	0.88
Erucic acid	-	22:1	$C_{22}H_{42}O_2$	338.58	-
Nervonic acid	-	24:1	$C_{24}H_{46}O_2$	366.63	-
cis-9, 12-Linoleic acid	Octadecadienoic acid	18:2	$C_{18}H_{32}O_2$	280.45	1.18
α-Linolenic acid	Octadecatrienoic acid	18:3	$C_{18}H_{30}O_2$	278.44	0.08
cis-11,14-Eicosadienoic acid	-	20:2	$C_{20}H_{36}O_2$	308.5	-
cis-11,14,17-Eicosadienoic acid	-	20:3	$C_{20}H_{34}O_2$	306.49	0.11
Docosahexaenoic acid	-	20:6	$C_{20}H_{28}O_2$	300.42	-

4.2.3 Product Analysis

The deoxygenation of beef fat over Al_2O_3-supported catalysts with different active metals was conducted at temperature of 325°C, reaction pressure of 500 psig, H_2/feed molar ratio of 30, and liquid hourly space velocity (LHSV) of 1 h^{-1}. A typical chromatogram of a liquid product from the reaction over Ni-Cu/Al_2O_3 catalyst is shown in Figure 4.7. In the chromatogram, pyridine and BSTFA were used as silylating agents, C_{20} in C_{12} were used as internal standards. The chromatogram consists of two main hydrocarbon peaks of n-pentadecane (n-C15), n-heptadecane (n-C17). Moreover, a chromatogram is mainly composed of feed remained and reaction intermediate peaks i.e. fatty alcohols, fatty acids, and fatty esters.

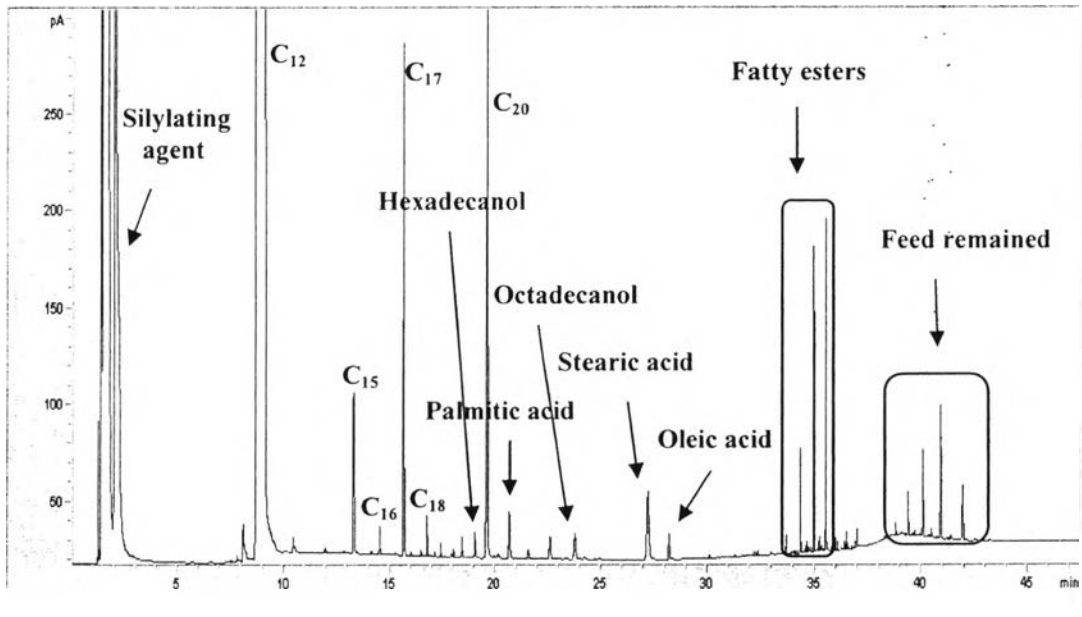

Figure 4.7 A typical chromatogram of liquid product (reaction condition: catalyst = Ni-Cu/Al_2O_3, temperature: 325 °C, pressure: 500 psig, H_2/feed molar ratio: 30, and TOS: 6 h).

4.3 Catalytic Activity Testing

To study the catalytic activity, selectivity and stability of the tested catalysts, the deoxygenation of beef fat was conducted at 325°C, 500 psig, liquid hourly space velocity (LHSV) of 1 h^{-1}, and H_2/feed molar ratio of 30.

4.3.1 Catalytic Activity over Ni-based Catalysts

4.3.1.1 Ni/Al_2O_3 Catalyst

Figure 4.8 shows the conversion and product selectivity over Ni/Al_2O_3 catalyst. The result showed that Ni/Al_2O_3 catalyst gave the products in diesel range with high selectivity towards n-heptadecane (n-C_{17}) followed by n-pentadecane (n-C_{15}). This is in agreement with the work done by Kubicka and Kaluza (2010).

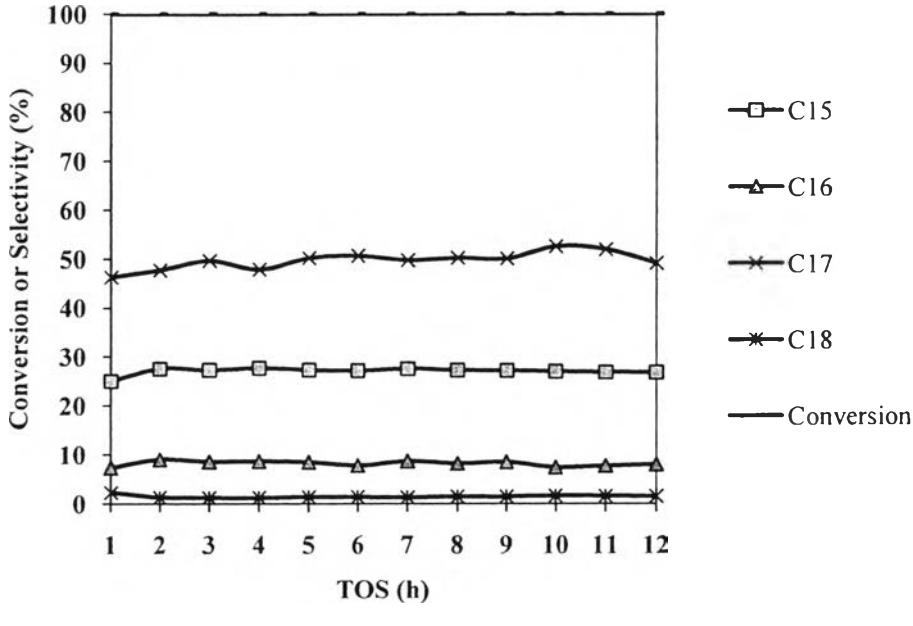

Figure 4.8 Conversion and product selectivity over Ni/Al_2O_3 catalyst. (Reaction conditions: T = 325 °C, P = 500 psig, LHSV = 1 h^{-1})

4.3.1.2 Ni-Mo/Al_2O_3 Catalyst

Figure 4.9 shows the conversion and product selectivity over Ni-Mo/Al_2O_3 catalyst. The Ni-Mo/Al_2O_3 catalyst showed high selectivity of hydeoxygenation pathway, resulted in high selectivity towards n-octadecane (n-C_{18}) followed by n-hexadecane (n-C_{16}).

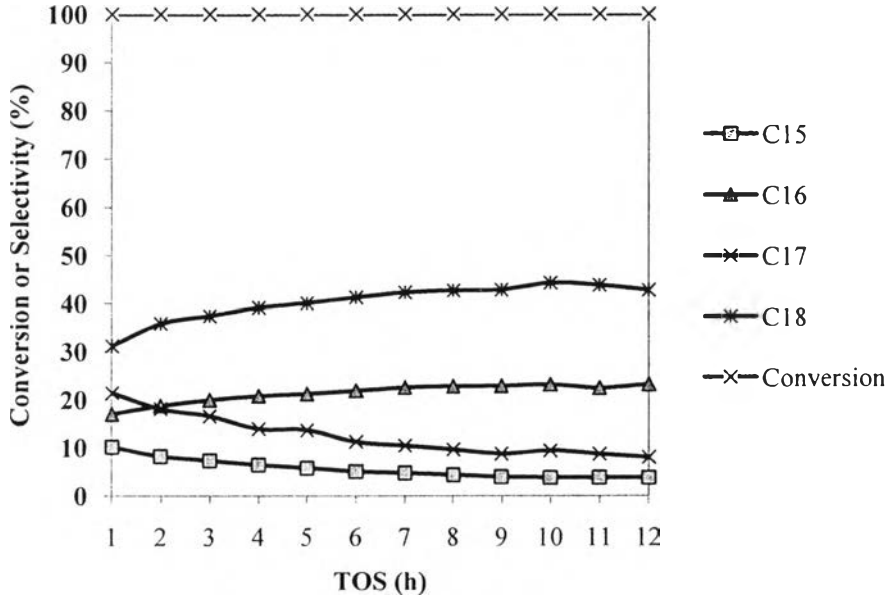

Figure 4.9 Conversion and product selectivity over Ni-Mo/Al_2O_3 catalyst. (Reaction conditions: T = 325 °C, P = 500 psig, LHSV = 1 h^{-1})

4.3.1.3 Ni-Co/Al_2O_3 Catalyst

Figure 4.10 shows the conversion and product selectivity over Ni-Co/Al_2O_3 catalyst. The Ni-Co/Al_2O_3 catalyst gave high selectivity towards n-haptadecane (n-C_{17}) followed by n-pentadecane (n-C_{15}). When the time on stream increased, selectivity to intermediates including palmitic acid, stearic acid increased.

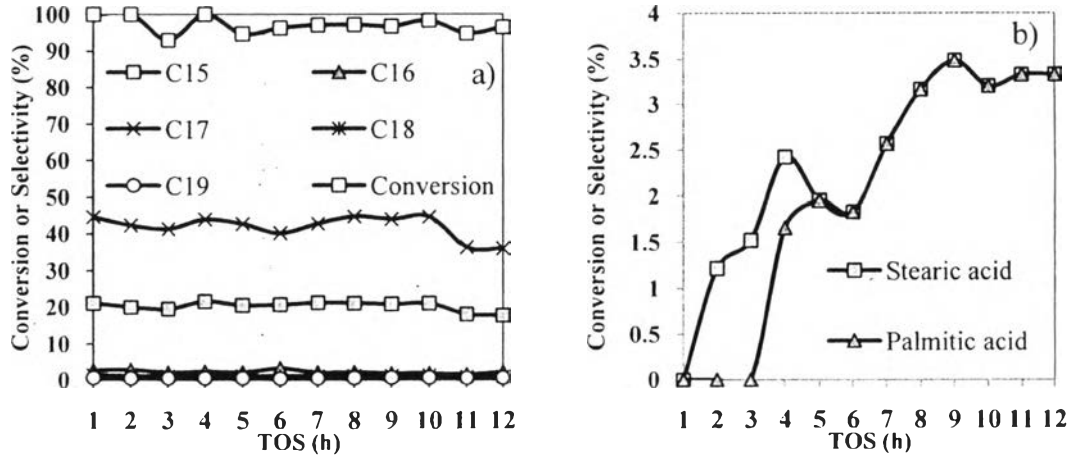

Figure 4.10 (a) Conversion and hydrocarbon selectivity and (b) intermediate selectivity over Ni-Co/Al_2O_3 catalyst. (Reaction conditions: T = 325 °C, P = 500 psig, LHSV = 1 h^{-1})

4.3.1.4 Ni-Cu/Al_2O_3 Catalyst

Figure 4.11 shows the conversion and product selectivity over Ni-Cu/Al_2O_3 catalyst. The Ni-Cu/Al_2O_3 catalyst gave high selectivity towards n-heptadecane (n-C_{17}) followed by diglyceride. The selectivity to intermediates, especially diglyceride increased with time on stream.

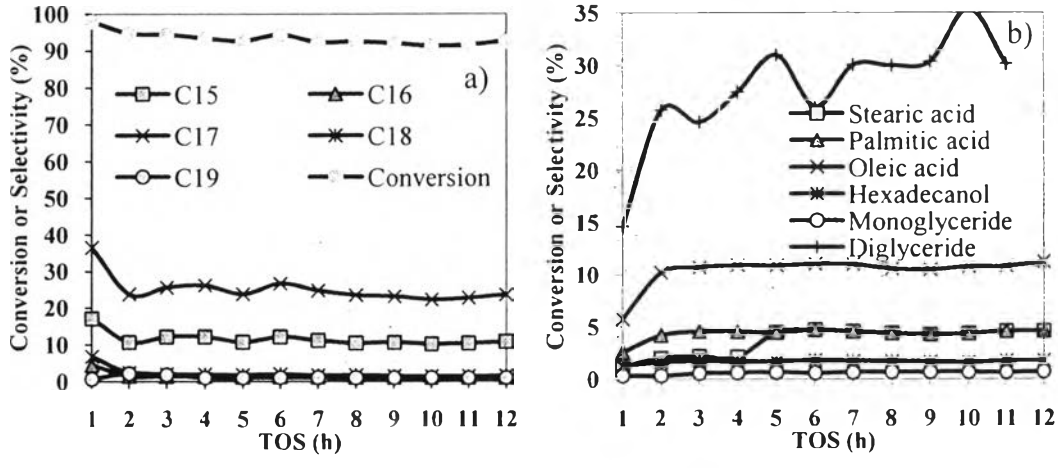

Figure 4.11 (a) Conversion and hydrocarbon selectivity and (b) intermediate selectivity over Ni-Cu/Al_2O_3 catalyst. (Reaction conditions: T = 325 °C, P = 500 psig, LHSV = 1 h^{-1})

4.3.1.5 Ni-W/Al_2O_3 Catalyst

Figure 4.12 shows the conversion and product selectivity over Ni-W/Al_2O_3 catalyst. The Ni-W/Al_2O_3 catalyst gave high selectivity towards n-octadecane (n-C_{18}) followed by n-haptadecane (n-C_{17}). The Ni-W/Al_2O_3 catalyst gave similar selectivity to products from both reaction pathways; hydrodeoygenation and hydrodecarboxylation. However, at this reaction condition, Ni-W/Al_2O_3 gave high amount of intermediates i.e. palmitic acid, stearic acid, and fatty esters.

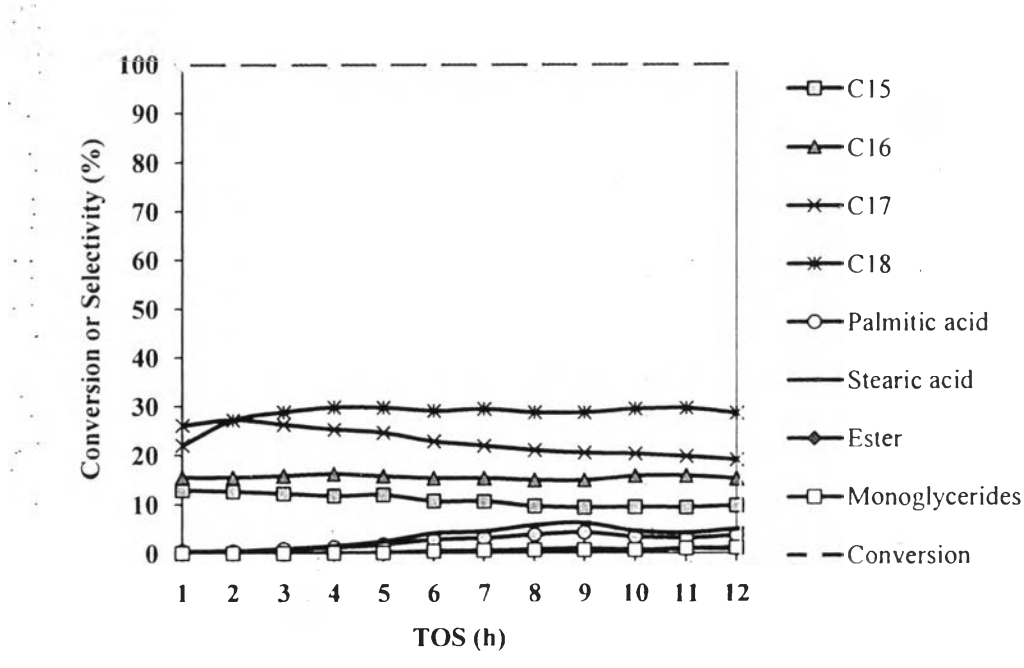

Figure 4.12 Conversion and product selectivity over Ni-W/Al_2O_3 catalyst. (Reaction conditions: T = 325 °C, P = 500 psig, LHSV = 1 h^{-1})

4.3.1.6 Ni-Ru/Al_2O_3 Catalyst

Figure 4.13 shows the conversion and product selectivity over Ni-Ru/Al_2O_3 catalyst. The Ni-Ru/Al_2O_3 catalyst gave high selectivity towards n-heptadecane (n-C_{17}) followed by n-pentadecane (n-C_{15}). When the time on stream increased, selectivity of intermediates including palmitic acid, oleic acid increased.

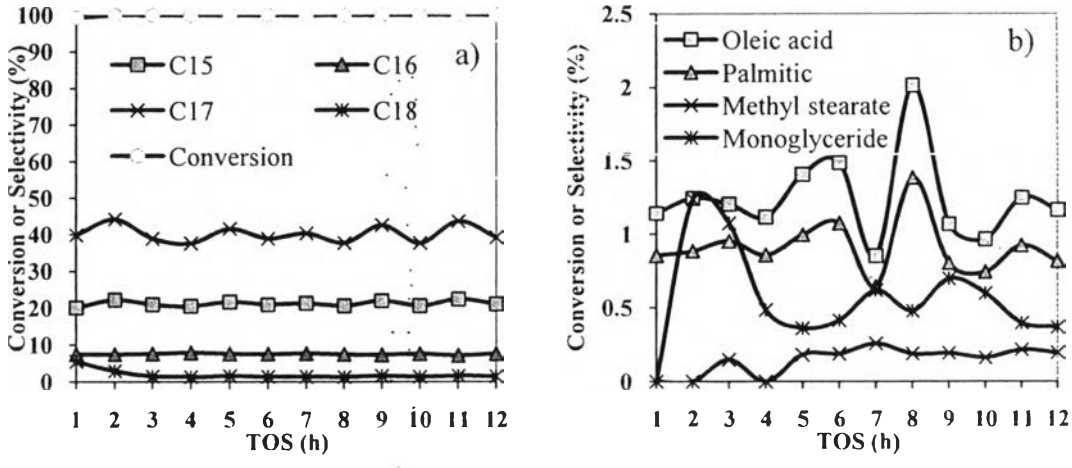

Figure 4.13 Conversion (a) Conversion and hydrocarbon selectivity and (b) intermediate selectivity over Ni-Ru/Al_2O_3 catalyst. (Reaction conditions: T = 325 °C, P = 500 psig, LHSV = 1 h^{-1})

4.3.1.7 Ni-Rh/Al_2O_3 Catalyst

Figure 4.14 shows the conversion and product selectivity over Ni-Rh/Al_2O_3 catalyst. The Ni-Rh/Al_2O_3 catalyst gave high selectivity towards n-heptadecane (n-C_{17}) followed by n-pentadecane (n-C_{15}). When the time on stream increased, selectivity of intermediates including palmitic acid, stearic acid increased.

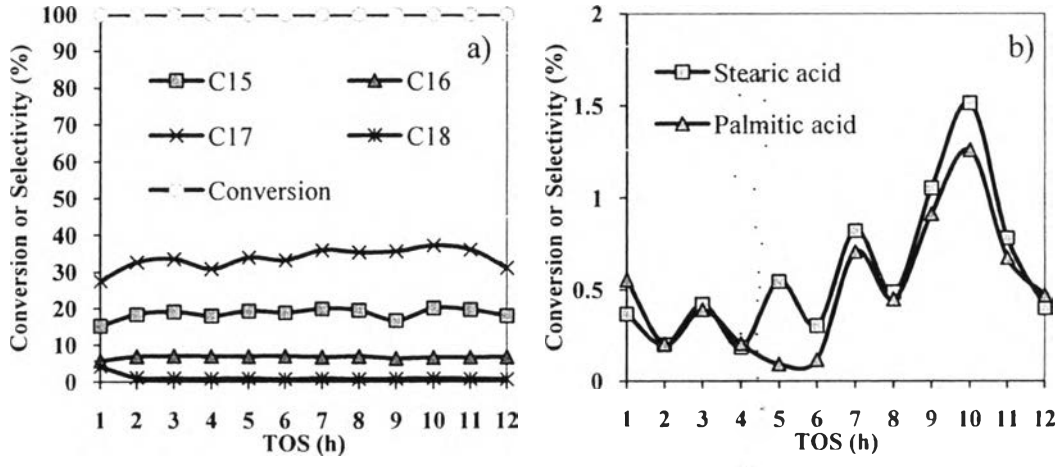

Figure 4.14 (a) Conversion and hydrocarbon selectivity and (b) intermediate selectivity over Ni-Rh/Al_2O_3 catalyst. (Reaction conditions: T = 325 °C, P = 500 psig, LHSV = 1 h^{-1})

4.3.1.8 Ni-Ir/Al_2O_3 Catalyst

Figure 4.15 shows the conversion and product selectivity over Ni-Ir/Al_2O_3 catalyst. The Ni-Ir/Al_2O_3 catalyst gave high selectivity towards n-heptadecane (n-C_{17}) followed by n-pentadecane (n-C_{15}). When the time on stream increased, selectivity of intermediates including palmitic acid, stearic acid, hexadecanol, and monoglycerides increased

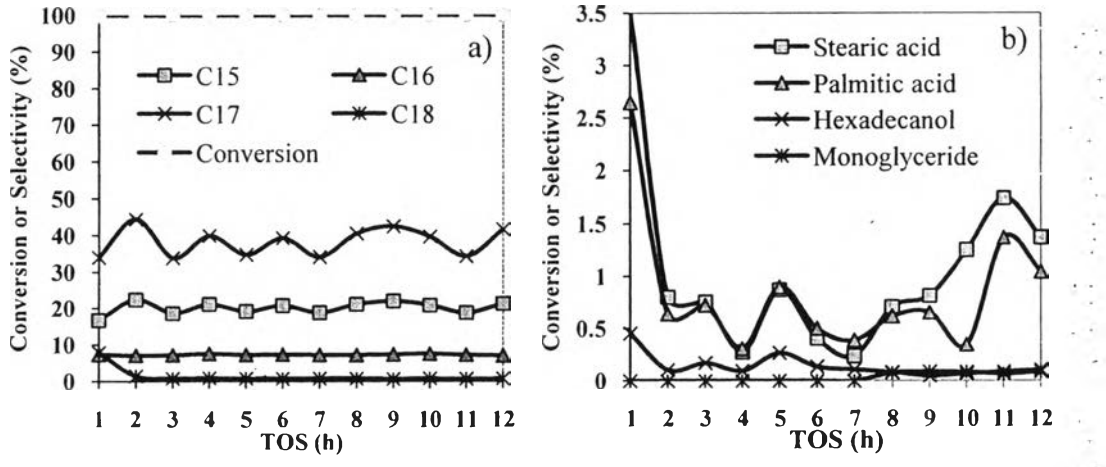

Figure 4.15 (a) Conversion and hydrocarbon selectivity and (b) intermediate selectivity over Ni-Ir/Al_2O_3 catalyst. (Reaction conditions: T = 325 °C, P = 500 psig, LHSV = 1 h^{-1})

4.3.2 Catalytic Activity over Cu-based Catalysts

4.3.2.1 Cu/Al_2O_3 Catalyst

Figure 4.16 shows conversion and product selectivity over Cu/Al_2O_3 catalyst. The result shows that Cu/Al_2O_3 catalyst gives the products in diesel range which high selectivity towards n-octadecane (n-C_{18}) followed by n-hexadecane (n-C_{16}) and intermediates as stearic acid, oleic acid, and palmitic acid together. When the time on stream increased, selectivity of n-octadecane and n-hexadecane drastically decreased while the selectivity of intermediates i.e. monoglycerides, diglycerides increased.

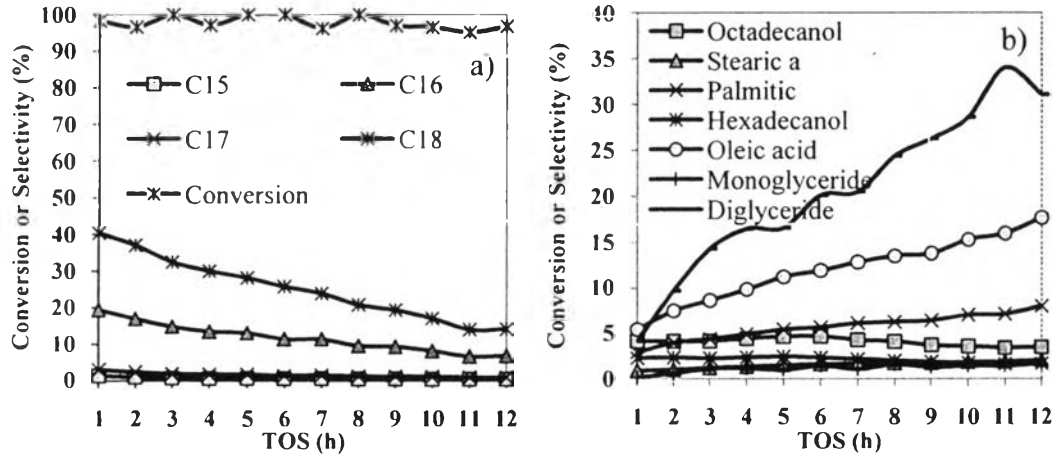

Figure 4.16 (a) Conversion and hydrocarbon selectivity and (b) intermediate selectivity over Cu/Al_2O_3 catalyst. (Reaction conditions: T = 325 °C, P = 500 psig, LHSV = 1 h^{-1})

4.3.2.2 Cu-Mo/Al_2O_3 Catalyst

Figure 4.17 shows conversion and product selectivity over Cu-Mo/Al_2O_3 catalyst. The result shows that Cu-Mo/Al_2O_3 catalyst gave products in diesel range with high selectivity towards n-octadecane (n-C_{18}) followed by n-hexadecane (n-C_{16}) and intermediates (stearic acid, oleic acid, and palmitic acid).

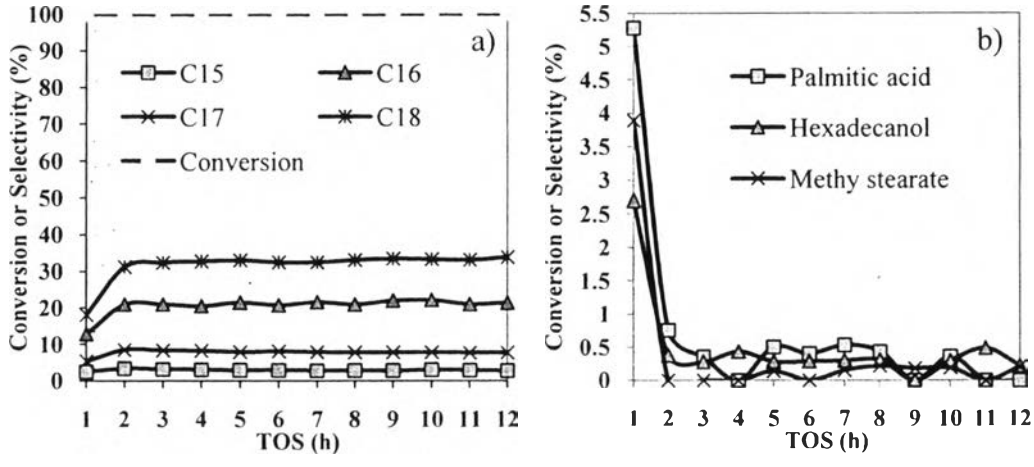

Figure 4.17 (a) Conversion and hydrocarbon selectivity and (b) intermediate selectivity over Cu-Mo/Al_2O_3 catalyst. (Reaction conditions: T = 325 °C, P = 500 psig, LHSV = 1 h^{-1})

4.3.2.3 Cu-Co/Al_2O_3 Catalyst

Figure 4.18 shows conversion and product selectivity over Cu-Co/Al_2O_3 catalyst. The result shows that Cu-Co/Al_2O_3 catalyst gave the products in diesel range which high selectivity towards n-heptadecane (n-C_{17}) followed by n-pentadecane (n-C_{15}) and much intermediates as hexadecanol, palmitic acid, and other intermediates together. When the time on stream increased, selectivity of fatty esters drastically increased. However, the selectivity of hydrodecarboxylation product (n-C_{17}, n-C_{15}) was drastically decreased while the selectivity of hydrodeoxygenation product slowly decreased until eight hour.

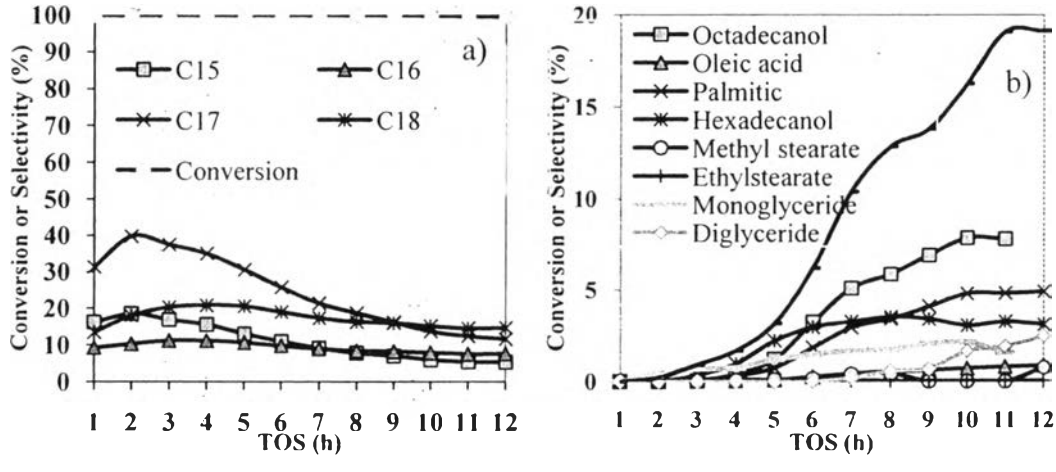

Figure 4.18 (a) Conversion and hydrocarbon selectivity and (b) intermediate selectivity over Cu-Co/Al_2O_3 catalyst. (Reaction conditions: T = 325 °C, P = 500 psig, LHSV = 1 h^{-1})

4.3.2.4 Cu-W/Al_2O_3 Catalyst

Figure 4.19 shows conversion and product selectivity over Cu-W/Al_2O_3 catalyst. The result shows that Cu-W/Al_2O_3 catalyst gave the products in oxygenated products which high selectivity towards palmitic acid followed by octadecanol and n-octadecane (n-C_{18}), respectively.

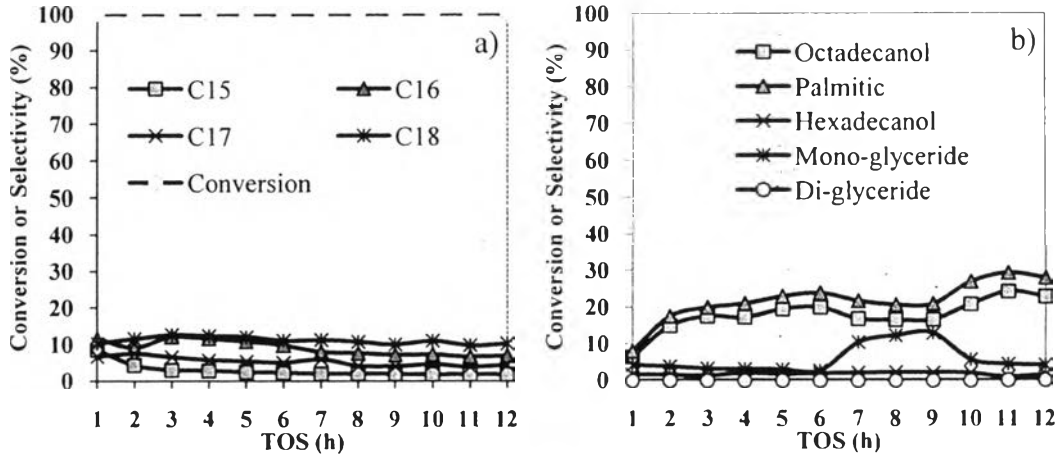

Figure 4.19 (a) Conversion and hydrocarbon selectivity and (b) intermediate selectivity over Cu-W/Al_2O_3 catalyst. (Reaction conditions: T = 325 °C, P = 500 psig, LHSV = 1 h^{-1})

4.3.2.5 Cu-Zn/Al_2O_3 Catalyst

Figure 4.20 shows conversion and product selectivity over Cu-Zn/Al_2O_3 catalyst. The result shows that Cu-Zn/Al_2O_3 catalyst gave the products in diesel range which high selectivity towards n-octadecane (n-C_{18}) followed by n-hexadecane (n-C_{16}) and intermediates as fatty esters together. When the time on stream increased, selectivity of fatty esters drastically increased while the selectivity of hydrodeoxygenation drastically decreased.

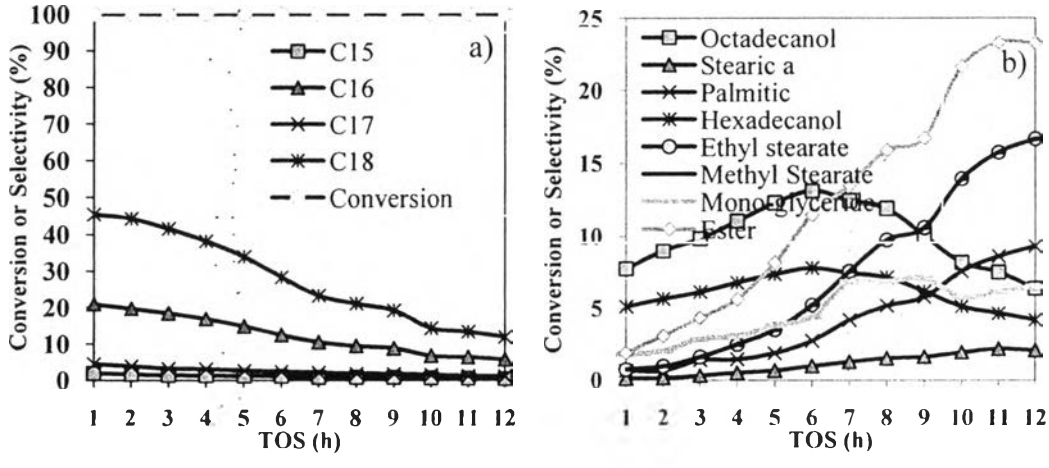

Figure 4.20 (a) Conversion and hydrocarbon selectivity and (b) intermediate selectivity over Cu-Zn/Al_2O_3 catalyst. (Reaction conditions: T = 325 °C, P = 500 psig, LHSV = 1 h^{-1})

4.3.3 Catalytic Activity over Noble Metal Catalysts

4.3.3.1 Pd/Al_2O_3 Catalyst

Figure 4.21 shows the conversion and product selectivity over Pd/Al_2O_3 catalyst. The result shows that Pd/Al_2O_3 catalyst gives the products in diesel range which high selectivity towards n-heptadecane (n-C_{17}) followed by n-pentadecane (n-C_{15}) and intermediates as oleic acid and palmitic acid.

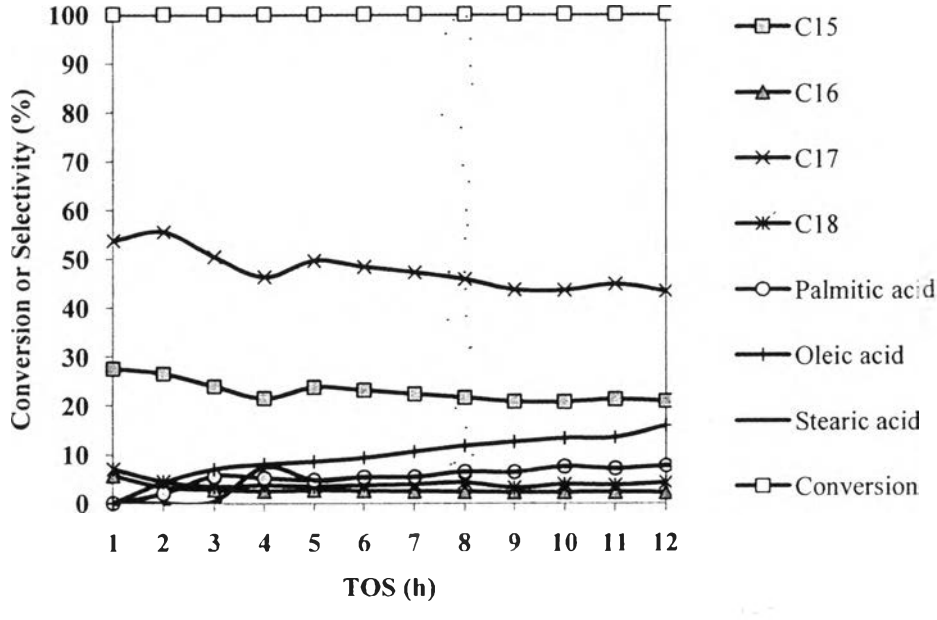

Figure 4.21 Conversion and product selectivity over Pt/Al_2O_3 catalyst. (Reaction conditions: T = 325 °C, P = 500 psig, LHSV = 1 h^{-1})

4.3.3.2 Pt/Al_2O_3 Catalyst

Figure 4.22 shows the conversion and product selectivity over Pt/Al_2O_3 catalyst. The result shows that Pt/Al_2O_3 catalyst gives the products in diesel range which high selectivity towards n-heptadecane (n-C_{17}) followed by n-pentadecane (n-C_{15}) and intermediates as oleic acid, palmitic acid, and diglyceride.

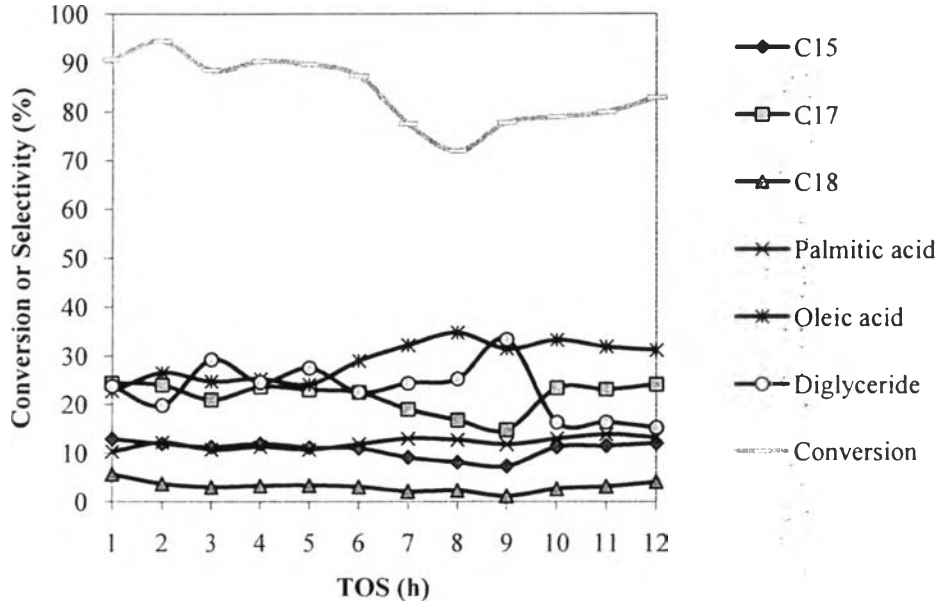

Figure 4.22 Conversion and product selectivity over Pt/Al_2O_3 catalyst. (Reaction conditions: T = 325 °C, P = 500 psig, LHSV = 1 h^{-1})

4.4 Overall Product Distribution

There are two main groups of liquid product obtained from deoxygenation reaction. The first group is hydrocarbons which mainly consist of n-pentadecane (n-C15), n-hexadecane (n-C16), n-heptadecane (n-C17), and n-octadecane (n-C18). The other group is oxygenates which are the reaction intermediates, i.e. fatty alcohols (hexadecanol and octadecanol), fatty acids (palmitic acid, oleic acid and stearic acid), fatty esters (methylstearate ethylstearate palmitylpalmitate, palmitylstearate, stearylpalmitate, and stearylstearate), and small amount of monoglycerides and diglycerides. The selectivity to hydrocarbons and oxygenated based on the total yield of liquid product and hydrocarbon yield behavior when time on stream increased are depicted in Table 4.6. Moreover, In addition, the yield to hydrocarbons of Ni-based catalysts is higher than that of other catalysts corresponding to the lower selectivity to oxygenates, except Cu-Mo/Al_2O_3. Moreover, small amount of isomerized hydrocarbons were detected, and no short chain liquid hydrocarbon were observed in this study.

Besides hydrocarbon and xygenated products, water was also detected. From liquid product, it can be seen that oxygen elimination from triglycerides proceeds via the formation of water. The formation of water corresponds to deoxygenation reaction carried out via hydrodexygenation pathway giving hydrocarbons with even number of carbon atoms in their molecules (corresponding to the number of carbon atoms of respective fatty acids bound in triglycerides) such as n-hexadecane and n-octadecane. On the other side, the formation of carbon dioxide and carbon monoxide relates to decarboxylation and decarbonylation, respectively yielding hydrocarbons with odd number of carbon atoms (one carbon atom less than in respective fatty acids) such as n-pentadecane and n-heptadecane.

Table 4.6 Hydrocarbon yield and oxygenated yield over prepared catalysts (Reaction conditions: T = 325 °C, P = 500 psig, LHSV = 1 h^{-1}, TOS = 6 h)

Prepared catalysts	Hydrocarbon yield (C_{15}-C_{18})	Oxygenated yield
Ni-based catalysts		
Ni	87.06	11.86
Ni-Mo	83.60	14.39
Ni-Co	62.71	30.26
Ni-Cu	39.86	49.27
Ni-W	85.69	14.31
Ni-Ru	72.47	27.53
Ni-Rh	62.31	37.69
Ni-Ir	70.06	29.94
Cu-based catalysts		
Cu	39.38	56.17
Cu-Mo	91.83	8.17
Cu-Co	70.32	29.68
Cu-W	37.56	62.08
Cu-Zn	48.98	49.86
Noble metal catalysts		
Pt	31.90	44.38
Pd	77.72	22.28

In order to compare hydrocarbon yield versus time on stream, the results showed that Ni/Al_2O_3, Ni-Mo/Al_2O_3, Ni-W/Al_2O_3, and Cu-Mo/Al_2O_3 gave yield over 80 % whole operating time. Moreover, most of Ni-based catalysts gave relatively constant hydrocarbon yield in length of operating time while Cu-based and noble metal catalysts gave hydrocarbon yield drastically decreased when time on stream increased, except Cu-Mo/ Al_2O_3. The results was shown in Figure 4.23- 4.25.

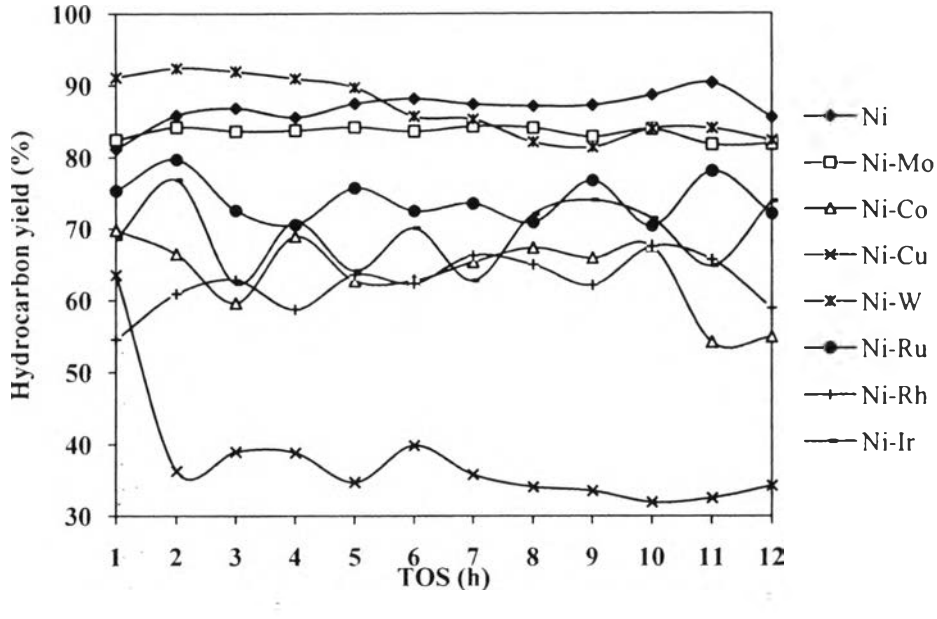

Figure 4.23 Hydrocarbon yield vs TOS over Ni-based catalysts (Reaction conditions: T = 325 °C, P = 500 psig, LHSV = 1 h^{-1}) .

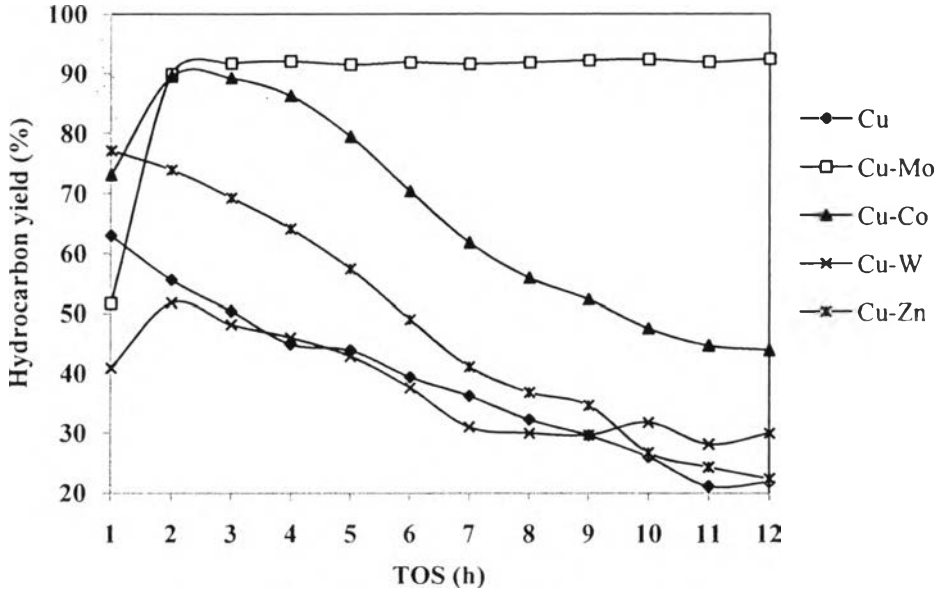

Figure 4.24 Hydrocarbon yield vs TOS over Cu-based catalysts (Reaction conditions: T = 325 °C, P = 500 psig, LHSV = 1 h^{-1}).

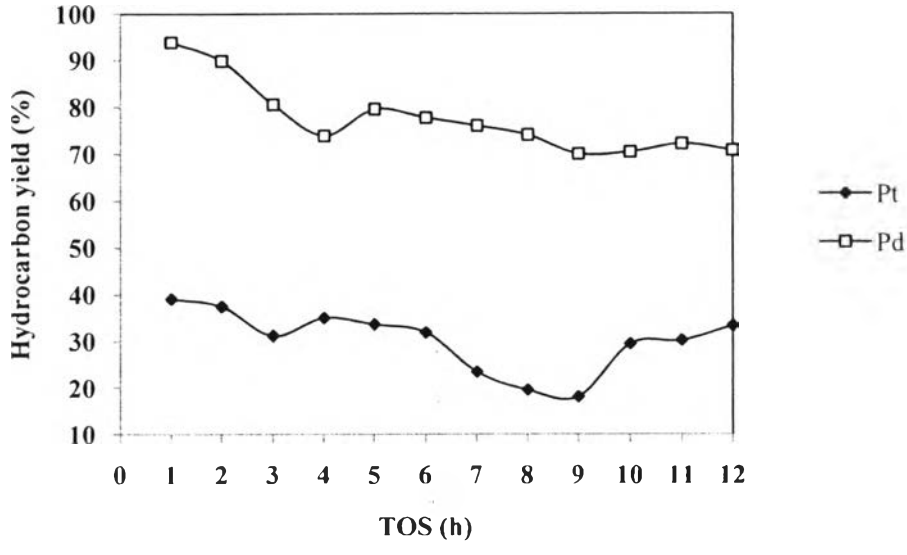

Figure 4.25 Hydrocarbon yield vs TOS over noble metal catalysts (Reaction conditions: T = 325 °C, P = 500 psig, LHSV = 1 h^{-1}).

4.4.1 Hydrocarbon Product Distribution

From the product distribution results, Ni-based catalysts prefer to select hydrodecarboxylation pathway that gave C15 and C17 as product, except Ni-Mo/Al_2O_3 and Ni-W/Al_2O_3. The results of hydrocarbon product distribution over Ni-based catalysts are shown in Figure 4.26 and 4.27. In case of Cu-based catalysts, Cu-based catalysts favored to select hydrodeoxygenation pathway, except Cu-Co/Al_2O_3 at the first hour. It showed in Figure 4.28 and 4.29. For noble metal, Pt/Al_2O_3 and Pd/Al_2O_3 evidently gave hydrodecarboxylation product as shown Figure 4.30 and4.31.

For selectivity to hydrodeoxyganation pathway, the Ni-Mo/Al_2O_3 and Ni-W/Al_2O_3 and Cu-Mo Al_2O_3 were the most interesting catalysts. On the other hand, Ni /Al_2O_3, Ni-Co/Al_2O_3, Ni-Rho/Al_2O_3 and Pd/Al_2O_3 were the fine catalysts that gave selectivity in hydrodecarboxylation pathway.

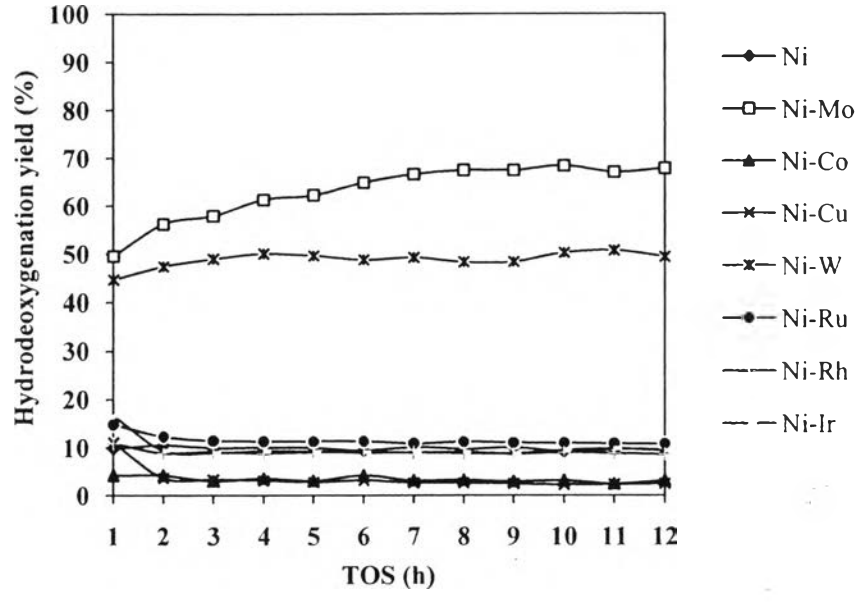

Figure 4.26 Hydrodeoxylation yield vs TOS over Ni-based catalysts.(Reaction conditions: T = 325 ºC, P = 500 psig, LHSV = 1 h^{-1}).

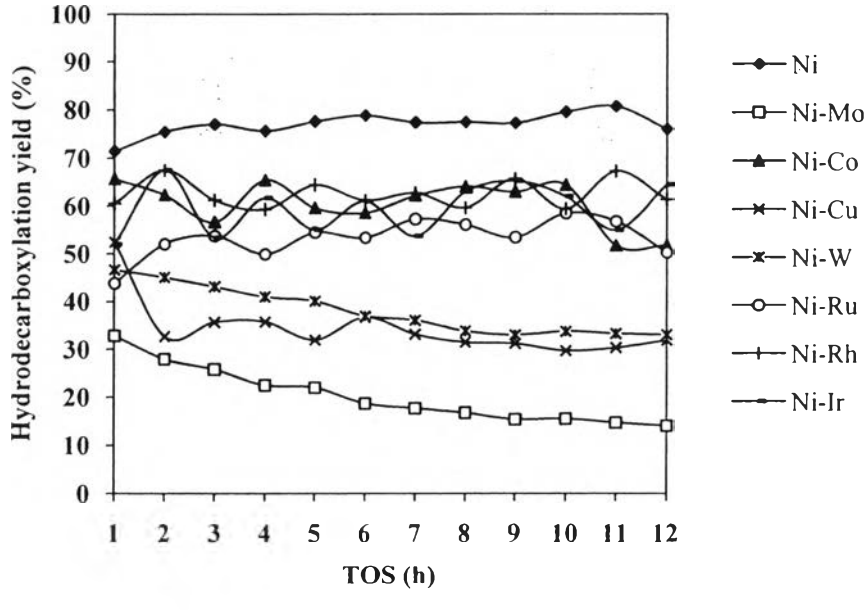

Figure 4.27 Hydrodecarboxylation yield vs TOS over Ni-based catalysts (Reaction conditions: T = 325 ºC, P = 500 psig, LHSV = 1 h^{-1}).

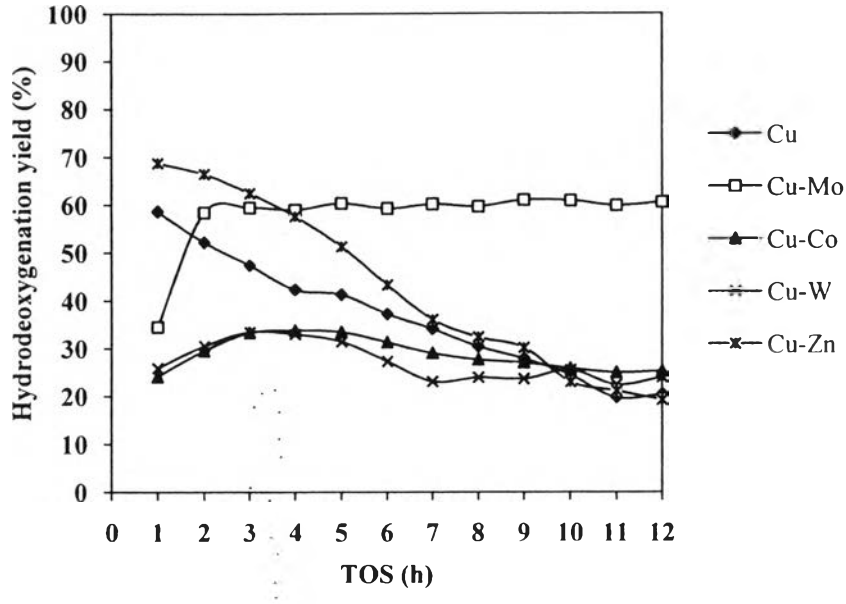

Figure 4.28 Hydrodeoxylation yield vs TOS over Cu-based catalysts (Reaction conditions: T = 325 °C, P = 500 psig, LHSV = 1 h^{-1}) .

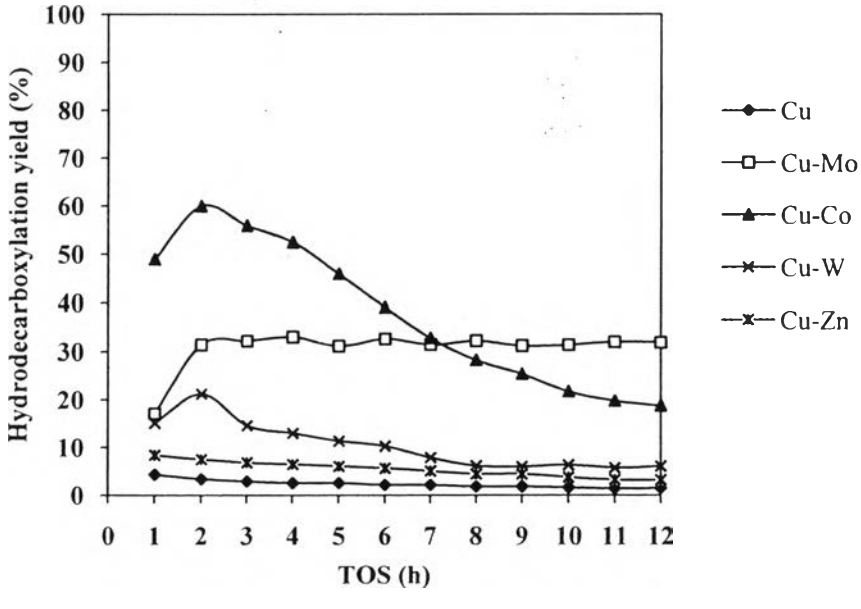

Figure 4.29 Hydrodecarboxylation yield vs TOS over Cu-based catalysts (Reaction conditions: T = 325 °C, P = 500 psig, LHSV = 1 h^{-1}).

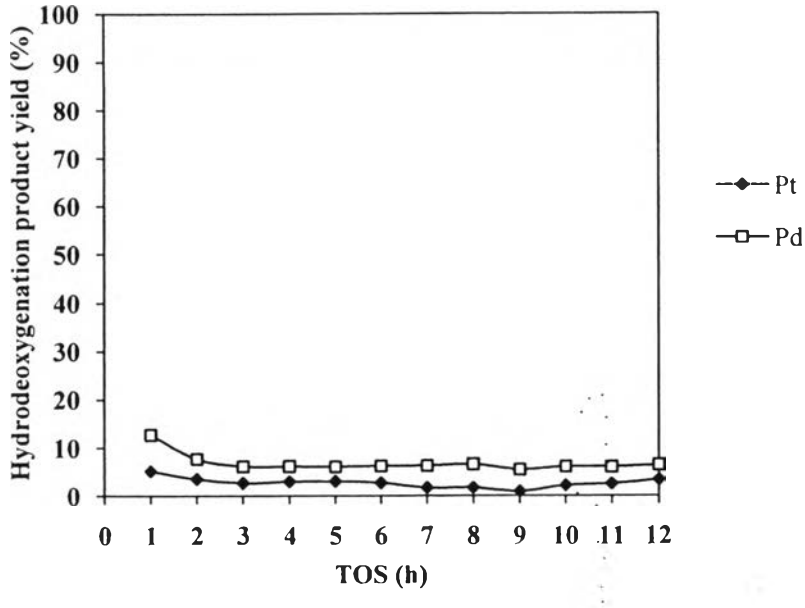

Figure 4.30 Hydrodeoxylation yield vs TOS over noble metal catalysts (Reaction conditions: T = 325 °C, P = 500 psig, LHSV = 1 h^{-1}) .

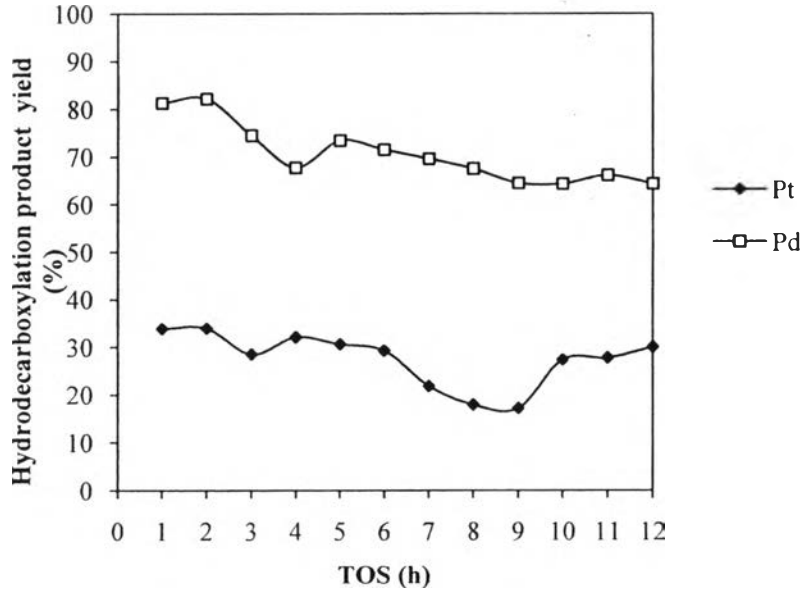

Figure 4.31 Hydrodecarboxylation yield vs TOS over noble metal catalysts (Reaction conditions: T = 325 °C, P = 500 psig, LHSV = 1 h^{-1}).

4.5 Carbon Deposition of Prepared Catalysts by Using Temperature Programmed Oxidation (TPO)

The prepared catalysts were test for its stability of the deoxygenation of beef fat in term of carbon (coke) deposition that was shown in Table 4.7. The TPO profiles of Ni-based, Cu-based catalysts are shown in Figures 4.32 and 4.33, respectively. All catalysts exhibited peak at 250-600 °C indicating that carbon deposit on metal surface. Moreover, peak can be attributed to reactive deposits, such as disordered, or amorphous deposits, and metal carbide particles. (Akin et al., 2000)

Coking of nickel-based catalysts is reasonably well described as, hydrocarbons dissociate on the metal surface to produce carbon deposits which are either gasified or dissolved in the nickel to produce coke. Although catalysts are not deactivated, pressure buildup in the reactor requires catalyst replacement. Avoidance of coking requires other metals that have been shown ability to control coking especially iridium (Trimm, 1997).

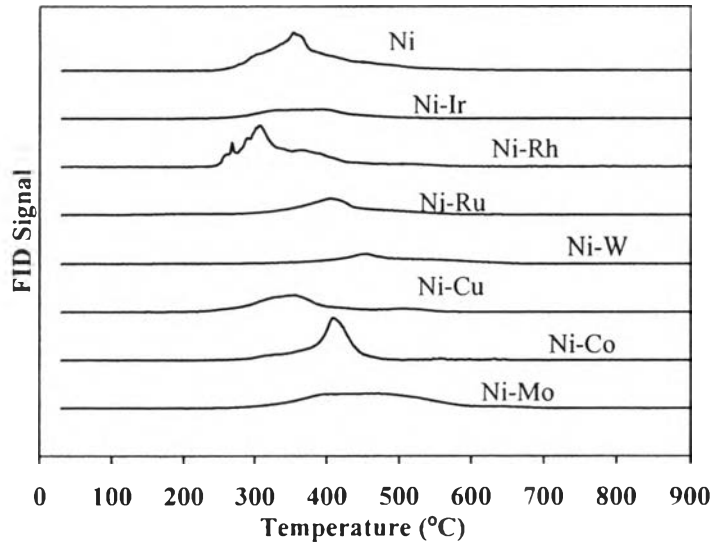

Figure 4.32 TPO patterns of spent Ni-based catalysts.

Coke formation on Cu-based catalysts is different. As would be expected, the morphology of the coke formed on copper was consistent with the formation of

gaseous encapsulating coke (Jackson et al., 1986) resulting that the catalyst activity were dropped rapidly.

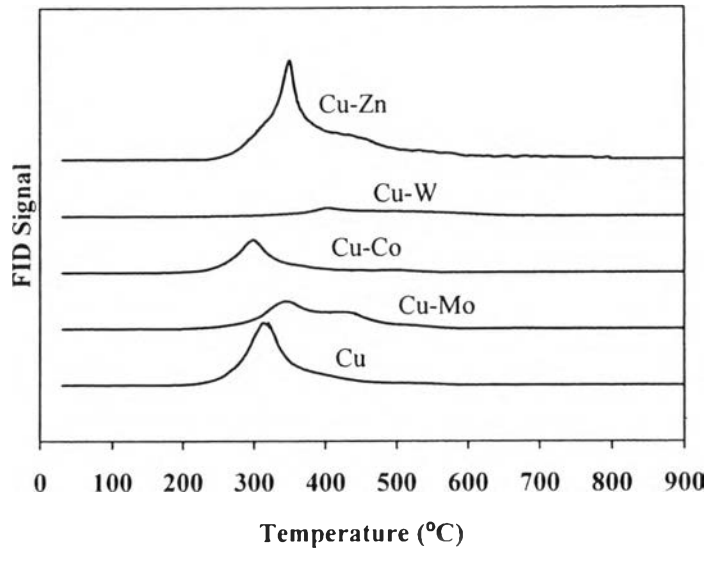

Figure 4.33 TPO patterns of spent Cu-based catalysts.

Table 4.7 Amount of coke deposit on prepared catalysts after reaction

Catalysts	Coke deposition (wt. %)
Ni-based catalysts	
Ni/Al_2O_3	43.15
$Ni-Mo/Al_2O_3$	20.84
$Ni-Co/Al_2O_3$	22.29
$Ni-Cu/Al_2O_3$	19
$Ni-W/Al_2O_3$	14.42
$Ni-Ru/Al_2O_3$	19.12
$Ni-Rh/Al_2O_3$	37.60
$Ni-Ir/Al_2O_3$	8.10
Cu-based catalysts	
Cu/Al_2O_3	32.52
$Cu-Mo/Al_2O_3$	25.69
$Cu-Co/Al_2O_3$	26.58
$Cu-W/Al_2O_3$	11.43
$Cu-Zn/Al_2O_3$	53.45
Noble catalysts	
Pt/Al_2O_3	34.03
Pd/Al_2O_3	10.50

In order to compare the overall catalytic activity or the performance of the studied catalysts, conversion of beef fat which mainly consists of triglyceride was determined. From Figure 4.8, the conversion of beef fat from the reaction over the investigated catalysts above 85%. From these results, it can be suggested that the deoxygenation of triglycerides is irreversible at the studied conditions which is in agreement a previous study. (Kubicka and Kaluza, 2010)

Most of Ni-based catalysts showed highly selective in hydrocarboxylation pathway that gave C_{17} and C_{15} as main product, except $Ni-Mo/Al_2O_3$ and $Ni-W/Al_2O_3$. The interesting catalysts in this group were Ni/Al_2O_3, $Ni-Mo/Al_2O_3$, Ni-

W/Al_2O_3 that gave high hydrocarbon yield. However, the monometallic Ni/Al_2O_3 had the highest carbon deposit (67 wt %) that cause decrease in catalytic activity at long operation time. In contrast, the addition of second metals showed much lower coke deposit. Therefore, the second metallic is useful for this reaction.

For Cu-based catalysts, $Cu\text{-}Mo/Al_2O_3$ was the most interesting one. It gave the highest hydrocarbon yield compared to other prepared catalysts. However, $Cu\text{-}Mo/Al_2O_3$ had high carbon deposit when compared to $Cu\text{-}W/Al_2O_3$

Noble catalysts gave high product in C_{15} and C_{17} especially Pd/Al_2O_3; nevertheless, Pt/Al_2O_3 had lowest conversion

Table 4.8 Catalyst composition, BET analysis, catalyst testing results, and coke analysis. (Reaction conditions: T = 325 °C, P = 500 psig, LHSV = 1 h^{-1}, TOS = 6 h)

Catalysts	Composition		S_{BET} (m^2/g)	Catalysts activity and selectivity				Coke deposition (wt. %)
	1st metal (wt.%)	2nd metal (wt.%)		Conversion (%)	Hydrocarbon (C_{15}-C_{18}) yield (%)	HDC/HDO*	Oxygenate (%)	
Ni-based catalysts								
Ni/Al_2O_3	10	-	218.9	100	87.06	8.44	11.86	43.15
$Ni\text{-}Mo/Al_2O_3$	10	5	148.1	100	83.60	0.26	14.39	20.84
$Ni\text{-}Co/Al_2O_3$	10	5	202.6	96.42	62.71	14.13	30.26	22.29
$Ni\text{-}Cu/Al_2O_3$	10	5	188.2	94.41	39.86	11.64	49.27	19
$Ni\text{-}W/Al_2O_3$	10	5	104.6	100	85.69	0.75	14.31	14.42
$Ni\text{-}Ru/Al_2O_3$	10	1	221.2	100	72.47	6.68	27.53	19.12
$Ni\text{-}Rh/Al_2O_3$	10	1	202.8	100	62.31	6.61	37.69	37.60
$Ni\text{-}Ir/Al_2O_3$	10	1	210.5	100	70.06	7.37	29.94	8.10
Cu-based catalysts								
Cu/Al_2O_3	10	-	228.4	97.18	39.38	0.06	56.17	32.52
$Cu\text{-}Mo/Al_2O_3$	10	5	202.9	100	91.83	0.21	8.17	32.82
$Cu\text{-}Co/Al_2O_3$	10	5	60.41	100	70.32	1.28	29.68	26.58
$Cu\text{-}W/Al_2O_3$	10	5	106	99.78	37.56	0.35	62.08	11.43
$Cu\text{-}Zn/Al_2O_3$	10	5	192.3	99.23	48.98	0.09	49.86	53.45
Noble catalysts								
Pt/Al_2O_3	1	-	246.5	87.34	31.90	31.90	44.38	34.03
Pd/Al_2O_3	1	-	243	100	77.72	75.95	22.28	10.50
Catalyst Support								
γ-alumina	-	-	235	-	-	-	-	-

* HDC = Hydrodecarboxylation yields C15, C17
HDO = Hydrodeoxygenation yields C16, C18